INSTITUTE OF PHYSICS PUBLISHING JOURNAL OF PHYSICS D: APPLIED PHYSICS

J. Phys. D: Appl. Phys. **40** (2007) 61–70 doi:10.1088/0022-3727/40/1/S10

# Single cell dielectric spectroscopy

**Hywel Morgan, Tao Sun, David Holmes, Shady Gawad[1] and Nicolas G Green**

Nanoscale Systems Integration Group, School of Electronics and Computer Science, University of Southampton, SO17 1BJ UK

E-mail: hm@ecs.soton.ac.uk

Received 1 September 2006
Published 15 December 2006
Online at stacks.iop.org/JPhysD/40/61

**Abstract**

Over the last century a number of techniques have been developed which allow the measurement of the dielectric properties of biological particles in fluid suspension. The majority of these techniques are limited by the fact that they only provide an average value for the dielectric properties of a collection of particles. More recently, with the advent of microfabrication techniques and the Lab-on-a-chip, it has been possible to perform dielectric spectroscopic experiments on single biological particles suspended in physiological media. In this paper we review current methods for single cell dielectric spectroscopy. We also discuss alternative single cell dielectric measurement techniques, specifically the ac electrokinetic methods of dielectrophoresis and electrorotation. Single cell electrical impedance spectroscopy is also discussed with relevance to a microfabricated flow cytometer. We compare impedance spectroscopy data obtained from measurements made using a microfabricated flow cytometer with simulation data obtained using an equivalent circuit model for the device.

## 1. Introduction

The dielectric properties of biological cells and tissues have been of interest for nearly a hundred years. The earliest work can be traced back to the 1910s, when Höber [1–3] compared the low and high frequency conductivity of erythrocytes (red blood cells-RBCs) and demonstrated the existence of the cellular membrane electrically. In 1924 and 1925 Fricke published a series of papers on the mathematical modelling of the electrical conductivity and capacity of disperse systems [4–12], using principles laid out by Maxwell [13]. From measurements of canine RBC Fricke calculated the membrane capacitance to be 8.1 mF m$^{-2}$, and determined the thickness of the membrane as 3.3 nm. In 1935, Fricke and Curtis [14] used complex impedance measurements to follow the lysis of mammalian erythrocytes. Around the same time, Cole [15, 16] utilized the Maxwell's mixture equation to derive the complex impedance for a single shelled cell in suspension. He proposed a constant phase angle (CPA) model for the cell membrane and derived the equation for the famous Cole–Cole plot [17]. Cole and Cole published several papers [18–20] on the electrical impedance of biological eggs (*Hipponoë, Asteria* and *Arbacia*). Single cell measurements were first made in 1937 when Curtis and Cole [21] developed a method to measure the transverse electrical impedance of a cell by embedding two electrodes into grooves in which a *Nitella* cell was placed. In 1938, the same authors [22] measured single eggs that were placed inside a capillary tube. Schwan pioneered broad-band dielectric measurements, extending the upper frequency limit to 1 GHz and measured a range of biological materials from cell suspensions to tissue [23], as well as identifying the three well known dispersions ($\alpha$, $\beta$ and $\gamma$) [24, 25].

Typically, in dielectric spectroscopy, the impedance of a biological suspension is measured using an ac excitation signal. The suspension is held in a measurement cell containing two, three or four electrodes. The current passing through the system is measured as a function of frequency to give the electrical properties of the particles in suspension. Currently, there are numerous approaches for the dielectric measurement of biological suspensions and several excellent reviews of the techniques are available in the literature [26–36].

Over the last 20 years more emphasis has been placed on the development of techniques for single particle analysis using ac electrokinetic methods, primarily electrorotation and dielectrophoresis. AC electrokinetics is the study of the behaviour of particles (movement and/or rotation) subjected to an ac electric field. Electrical forces act on both the particles

[1] Present address: LMIS4-STI-EPFL, Swiss Federal Institute of Technology, 1015 Lausanne, Switzerland.

  

and the suspending fluid and have their origin in the charge and electric field distribution in the system. In general, particles such as cells do not have fixed dipole moments; in an electric field an induced dipole is formed by interfacial polarization. If the field is non-uniform a force is exerted on the dipole causing movement of the particle. If the particle is in a rotating field, the dipole continually tries to align itself with the field, resulting in a torque on the particle, which then rotates; a phenomenon known as electrorotation (ROT). For more details on the forces in ac electrokinetic systems see [33, 37, 38]. The torque and force depend on the dipole moment of the particle, and as a result measurement of either the particle linear or angular velocity can be used to measure the particle polarizability.

In this paper, we discuss the background and theory behind the techniques available for single cell dielectric spectroscopy. We present the design of a microfluidic cytometer for the high throughput analysis of single particles. The modelling of the system using Maxwell's mixture theory is discussed and compared with an equivalent circuit model (ECM). Experimental results from the system are then compared with PSpice simulation.

## 2. Theory

### *2.1. Dielectrophoresis (DEP)*

When an external electric field is imposed on a particle in suspension, provided the particle has different dielectric properties to the suspending medium, it will polarize by interfacial or Maxwell–Wagner polarization. The interaction between the induced dipole moment and the imposed electric field determines the dielectrophoretic force on the particle. In an ac field, the time-averaged DEP force $\langle F_{\mathrm{DEP}}\rangle$ is given by [28, 33]

$$\langle F_{\mathrm{DEP}}\rangle = \pi\varepsilon_{\mathrm{m}}R^3\mathrm{Re}[\tilde{f}_{\mathrm{CM}}]\Delta|\boldsymbol{E}|^2 \tag{1}$$

with the Clausius–Mossotti factor, given by

$$\tilde{f}_{\mathrm{CM}} = \frac{\tilde{\varepsilon}_{\mathrm{p}} - \tilde{\varepsilon}_{\mathrm{m}}}{\tilde{\varepsilon}_{\mathrm{p}} + 2\tilde{\varepsilon}_{\mathrm{m}}}, \tag{2}$$

where $R$ is the radius of the particle, $\boldsymbol{E}$ the electric field, Re[] represents the real part, and $\tilde{\varepsilon}_{\mathrm{p}}$ and $\tilde{\varepsilon}_{\mathrm{m}}$ are the complex permittivities of the particle and medium. In general the complex permittivity of a material is given by

$$\tilde{\varepsilon} = \varepsilon - \mathrm{j}\frac{\sigma}{\omega}, \tag{3}$$

where $\varepsilon$ is the permittivity, $\sigma$ the conductivity, $\mathrm{j}^2 = -1$ and $\omega$ the angular frequency.

According to equation (1), if the electric field is uniform, the gradient of the magnitude of the field is zero ($\nabla|\boldsymbol{E}|^2 = 0$), which means that there is no DEP force. The frequency dependence and the direction of the DEP force are governed by the real part of the Clausius–Mossotti factor. If the particle is more polarizable than the medium, ($\mathrm{Re}[\tilde{f}_{\mathrm{CM}}] > 0$), the particle is attracted to the high intensity electric field regions, this is termed positive dielectrophoresis (pDEP). Conversely if the particle is less polarisable than the medium, ($\mathrm{Re}[\tilde{f}_{\mathrm{CM}}] < 0$), the particle is repelled from the high intensity field regions and negative dielectrophoresis (nDEP) occurs.

In practice, it is difficult to measure the DEP force directly due to the effects of Brownian motion and electrically induced fluid flow [39]. Instead, the DEP crossover frequency [39–41] can be measured as a function of medium conductivity and provides sufficient information to determine the dielectric properties of the suspended particles.

The DEP crossover frequency is the transient frequency point where the DEP force switches from pDEP to nDEP or *vice versa*. According to equation (1), the crossover frequency is defined to be the frequency point that the real part of the Clausius–Mossotti factor equals zero:

$$f_{\mathrm{cross}} = \frac{1}{2\pi}\sqrt{\frac{(\sigma_{\mathrm{m}} - \sigma_{\mathrm{p}})(\sigma_{\mathrm{p}} + 2\sigma_{\mathrm{m}})}{(\varepsilon_{\mathrm{p}} - \varepsilon_{\mathrm{m}})(\varepsilon_{\mathrm{p}} + 2\varepsilon_{\mathrm{m}})}} = \frac{1}{\sqrt{2\pi}}\sqrt{\frac{\sigma_{\mathrm{m}} - \sigma_{\mathrm{p}}}{\varepsilon_{\mathrm{p}} - \varepsilon_{\mathrm{m}}}}f_{\mathrm{MW}} \tag{4}$$

with

$$f_{\mathrm{MW}} = \frac{1}{2\pi\,\tau_{\mathrm{MW}}} \tag{5}$$

$$\tau_{\mathrm{MW}} = \frac{\varepsilon_{\mathrm{p}} + 2\varepsilon_{\mathrm{m}}}{\sigma_{\mathrm{p}} + 2\sigma_{\mathrm{m}}}, \tag{6}$$

where $f_{\mathrm{cross}}$ is the crossover frequency, $f_{\mathrm{MW}}$ is the Maxwell–Wagner relaxation frequency and $\tau_{\mathrm{MW}}$ is the Maxwell–Wagner time constant characterizing the $\beta$-relaxation typically in a low MHz frequency range. Equation (4) shows the relationship between the crossover frequency and the Maxwell–Wagner relaxation frequency. Using a simplified shell model for a biological cell, the crossover frequency can be written in terms of the membrane capacitance and conductance of the cell [42]:

$$f_{\mathrm{cross}} = \frac{\sqrt{2}}{8\pi RC_{\mathrm{mem}}}\sqrt{(4\sigma_{\mathrm{m}} - RG_{\mathrm{mem}})^2 - 9R^2G_{\mathrm{mem}}^2}, \tag{7}$$

where $R$ is the radius of the cell and $C_{\mathrm{mem}}$ and $G_{\mathrm{mem}}$ are the specific capacitance and conductance of the membrane, respectively.

In addition to measurement of the crossover frequency, the DEP-induced particle velocity can be measured as a useful dielectric spectroscopy technique. The DEP induced particle velocity is directly proportional to the DEP force [33, 38, 43]:

$$u = \frac{F_{\mathrm{DEP}}}{6\pi R\eta} + \left(u_0 - \frac{F_{\mathrm{DEP}}}{6\pi R\eta}\right)\mathrm{e}^{-t/\tau}, \tag{8}$$

where $u$ is the DEP-induced velocity of the particle, $\eta$ is the viscosity if the suspension medium and $u_0$ is the initial velocity. The time constant $\tau$ is referred to as the momentum relaxation time and is given by

$$\tau = \frac{m}{6\pi R\eta}, \tag{9}$$

where $m$ is the mass of the particle. For a typical cell the momentum relaxation time is of the order of tens of microseconds. The practical application of DEP for manipulation, separation and selection of cells, beads, bacteria and viruses has been reported by a number of authors [44–49].

### *2.2. Electrorotation (ROT)*

The interaction of an electric field with a polarized particle creates an induced dipole moment. In a rotating electric field,

a torque is exerted on the induced dipole which causes the particle to rotate. The time-averaged torque is given by [33, 50]

$$\Gamma_{\mathrm{ROT}} = -4\pi\varepsilon_{\mathrm{m}} R^3 \mathrm{Im}[\tilde{f}_{\mathrm{CM}}]|\boldsymbol{E}|^2, \tag{10}$$

where Im[ ] indicates the imaginary part.

Equation (10) shows that the frequency-dependent property of the ROT torque depends on the imaginary part of the Clausius–Mossotti factor. The particle will rotate with or against the electric field, due to whether the imaginary part of the Clausius-Mossotti factor (Im[$\tilde{f}_{\mathrm{CM}}$]) is negative or positive. The ROT torque is measured indirectly by analysis of the rotation rate (angular velocity) of the particle, which is given by [33, 51]

$$R_{\mathrm{ROT}}(\omega) = -\frac{\varepsilon_{\mathrm{m}}\mathrm{Im}[\tilde{f}_{\mathrm{CM}}]|\boldsymbol{E}|^2}{2\eta} K, \tag{11}$$

where $R_{\mathrm{ROT}}(\omega)$ is the rotation rate and $K$ is a scaling factor. Again owing to the viscous nature of the system the momentum relaxation time is small resulting in a constant angular velocity proportional to the torque. ROT has been used widely to measure the dielectric properties of a variety of biological particles [52–57].

The frequency spectra of both the DEP force and ROT torque can provide significant information on the dielectric properties of biological particles in suspension. Separating the real and imaginary components of equation (2) gives

$$\mathrm{Re}[\tilde{f}_{\mathrm{CM}}] = \frac{(\sigma_{\mathrm{p}} - \sigma_{\mathrm{m}})}{(1+\omega^2\tau_{\mathrm{MW}}^2)(\sigma_{\mathrm{p}} + 2\sigma_{\mathrm{m}})} + \frac{\omega^2\tau_{\mathrm{MW}}^2(\varepsilon_{\mathrm{p}} - \varepsilon_{\mathrm{m}})}{(1+\omega^2\tau_{\mathrm{MW}}^2)(\varepsilon_{\mathrm{p}} + 2\varepsilon_{\mathrm{m}})} \tag{12}$$

$$\mathrm{Im}[\tilde{f}_{\mathrm{CM}}] = \frac{3\omega\tau_{\mathrm{MW}}(\varepsilon_{\mathrm{p}}\sigma_{\mathrm{m}} - \varepsilon_{\mathrm{m}}\sigma_{\mathrm{p}})}{(1+\omega^2\tau_{\mathrm{MW}}^2)(\varepsilon_{\mathrm{p}} + 2\varepsilon_{\mathrm{m}})(\sigma_{\mathrm{p}} + 2\sigma_{\mathrm{m}})}. \tag{13}$$

The relationship between DEP and ROT can be examined using Argand diagrams, where the real and imaginary parts of the Clausius–Mossotti factor are mapped onto the complex plane as a function of frequency. For further details on the theoretical relationship between DEP, ROT and dielectric spectroscopy see [43, 58–63].

### *2.3. Electrical impedance spectroscopy (EIS)*

In impedance spectroscopy, the dielectric properties of a system are determined by applying a frequency-dependent excitation signal and measuring the response. Conventionally, a small ac voltage, $\tilde{U}(\mathrm{j}\omega)$, over a range of frequencies is used as the excitation signal. The electrical current response, $\tilde{I}(\mathrm{j}\omega)$, is measured and the complex impedance $\tilde{Z}(\mathrm{j}\omega)$ of the system is

$$\tilde{Z}(\mathrm{j}\omega) = \frac{\tilde{U}(\mathrm{j}\omega)}{\tilde{I}(\mathrm{j}\omega)} = \tilde{Z}_{\mathrm{RE}} + \mathrm{j}\tilde{Z}_{\mathrm{IM}}. \tag{14}$$

Here $\tilde{Z}_{\mathrm{RE}}$ and $\tilde{Z}_{\mathrm{IM}}$ are the real and imaginary parts of the complex impedance, respectively. The real part is called resistance while the imaginary part is called reactance. The magnitude and phase angle of the complex impedance are

$$|\tilde{Z}| = \sqrt{\tilde{Z}_{\mathrm{RE}}^2 + \tilde{Z}_{\mathrm{IM}}^2} \tag{15}$$

and

$$\angle\tilde{Z} = \arctan\left(\frac{\tilde{Z}_{\mathrm{IM}}}{\tilde{Z}_{\mathrm{RE}}}\right), \tag{16}$$

respectively.

In this paper we use the term impedance spectroscopy, because the electrical response of the system is measured, rather than the properties of the single cell.

For a dilute suspension of particles, the impedance of the system is well described by Maxwell's mixture equation [64]. The equivalent complex permittivity of the mixture containing the particle and the suspending medium is given by

$$\tilde{\varepsilon}_{\mathrm{mix}} = \tilde{\varepsilon}_{\mathrm{m}} \frac{1 + 2\Phi\tilde{f}_{\mathrm{CM}}}{1 - \Phi\tilde{f}_{\mathrm{CM}}}, \tag{17}$$

where $\tilde{\varepsilon}_{\mathrm{mix}}$ is the complex permittivity of the mixture and $\Phi$ is the volume fraction (ratio of the particle volume to the detection volume).

The complex impedance of the system, $\tilde{Z}_{\mathrm{mix}}$, is then given by

$$\tilde{Z}_{\mathrm{mix}} = \frac{1}{\mathrm{j}\omega\tilde{C}_{\mathrm{mix}}}, \tag{18}$$

where $\tilde{C}_{\mathrm{mix}}$ is the complex capacitance of the system.

Measurement of the complex impedance of a suspension of particles can be used to derive the average dielectric properties of the particles.

In DEP and ROT, the polarizability of individual particles is measured directly; there is therefore no requirement to consider the volume fraction [65, 66]. However, the limitations of DEP and ROT are obvious. Measurement of DEP force or ROT torque gives the real or imaginary parts of the Clausius–Mossotti factor, respectively, so that in order to uniquely measure a cell, both the electrorotation spectrum and the DEP properties (crossover) have to be measured [67]. The other major limitation of these techniques is that of speed. A typical ROT assay takes several seconds per cell (usually longer). This means that a limited number of cells are measured, and temporal variations in cell behaviour are very difficult to monitor.

Impedance spectroscopy by contrast is fast and gives the complex dielectric properties very quickly. However, until recently the technique could only be used to measure the properties of large numbers of cells in a suspension. Recently, new instrumentation techniques, coupled with microfluidics [68] have led to novel systems for measurement of the dielectric properties of single cells at high speed [69, 70].

## 3. Microfluidic cytometry

Flow cytometry is a technique in which the properties of large numbers of cells are measured at high speed, one cell at a time. The technique has been widely used in the area of blood analysis for identification of different cell types. The first cytometer capable of measuring the electrical properties of single cells, was developed by Coulter [71]. The device measures the dc resistance between two electrically isolated fluid-filled chambers as cells pass through a small connecting orifice. For a fixed sized orifice, the change in electrical current can be used to count and size the cells. Further developments

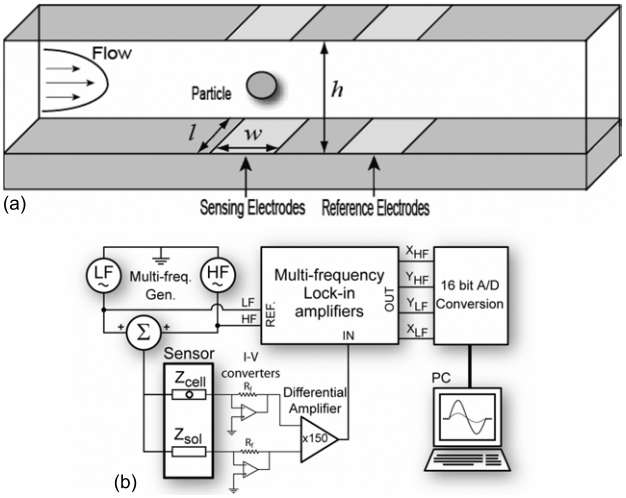


**Figure 1.** (*a*) Schematic of the microfluidic device showing the channel and detection electrodes. As a particle passes through the device it disrupts the electric field between the pairs of electrodes resulting in a measurable current flow. $w$ is the width and $l$ the length of the electrodes and $h$ is the height of the channel. (*b*) Schematic of the experimental set-up showing the detection electrodes and associated amplification and detection circuitry.

have used ac signals at high frequencies to give information on cell properties as well as cell volume [72, 73].

Recent developments in the field of microfabrication have led to the development of integrated systems generally known as the Lab-on-a-chip (LOAC). Advances in this field have led to micro-devices that can measure the properties of single cells in a manner analogous to commercial flow cytometers. Different designs of micro-cytometers have been fabricated capable of measuring the optical and/or the electrical properties of single particles [68–70, 74–84].

### *3.1. System setup*

We have developed a system that can measure the impedance properties of cells one at a time and at high speed. The microfabricated cytometer is shown in figure 1(*a*). The microchip is fabricated from glass and the electrodes are made from platinum. Microfluidic channels are made from polymers such as SU8 and polyimide. The chip is mounted in a custom holder that provides fluidic and electrical interconnects. The micro-channel has a cross-section of $20 \times 20\,\mu\text{m}^2$ and the electrodes have width and gap of $20\,\mu$m for further details see [80].

The sizes of the channel and electrode are chosen to optimize the sensitivity of the devices for the particular particle of interest. In order to obtain the maximum signal, the volume fraction of the cell has to be large, cf equation (17). Therefore, in order to measure cells, such as white blood cells which are typically 8–10 $\mu$m in diameter, the channel size is made $20\,\mu$m across. Figure 1(*b*) shows further details of the experimental system.

In the most general configuration, a number of individual ac signals are mixed and applied to the top microelectrodes—each signal representing a single probe frequency that is applied continuously. The signals generate an electric field in the channel, and when a cell passes through the device the electric field is perturbed, causing a change in the current. This current change is measured in differential mode, using two closely positioned detection volumes defined by the two pairs of electrodes as shown in figure 1(*a*). As a cell passes through the electrode gap, one pair is used for sensing the current change, whilst the other pair provides the reference. The change in electric current depends upon the size, shape and dielectric properties of the particle through the change in impedance of the detection area. The electronic circuit consists of a pair of current to voltage ($I$–$V$) converters followed by a differential amplifier. RF lock-in amplifiers (SR844, Stanford Research Systems) were used to demodulate the signals, giving the in-phase and out-of phase signals at each discrete frequency; and rejecting noise at all other frequencies. Data is collected with a 16 bit data acquisition card (National Instruments, USA). The bandwidth of the present system is 10 MHz. Data analysis was performed using software written in MATLAB™ (Mathworks Inc., Natick, MA, USA) which records the data and calculates parameters such as magnitude and phase.

### *3.2. Modelling and simulation*

Several approaches have been used to model the dielectric properties of single particles in suspension, including the finite element method [80], Maxwell's mixture theory (MMT) [33, 80, 85], equivalent circuit model (ECM) [27, 86], the boundary element method [87], the transport lattice method [88, 89] and the finite difference method [90]. In this work we used the MMT and ECM to simulate the impedance spectrum and electrical response of the particle in suspension.

In dielectric spectroscopy of cells, MMT (equation (17)) is generally used to obtain the dielectric properties of the individual components using the shell model to represent the particle. For a single shelled cell model, the complex permittivity of the cell is given by

$$\tilde{\varepsilon}_\text{p} = \tilde{\varepsilon}_\text{mem} \frac{\gamma^3 + 2\left(\dfrac{\tilde{\varepsilon}_\text{i} - \tilde{\varepsilon}_\text{mem}}{\tilde{\varepsilon}_\text{i} + 2\tilde{\varepsilon}_\text{mem}}\right)}{\gamma^3 - \left(\dfrac{\tilde{\varepsilon}_\text{i} - \tilde{\varepsilon}_\text{mem}}{\tilde{\varepsilon}_\text{i} + 2\tilde{\varepsilon}_\text{mem}}\right)} \tag{19}$$

with $\gamma = R/(R-d)$, $R$ is the radius of the cell, $d$ the thickness of the cell membrane and $\tilde{\varepsilon}_\text{i}$ and $\tilde{\varepsilon}_\text{mem}$ are the complex permittivities of the cytoplasm and the membrane, respectively.

Mixture theory works well for low volume fractions and in a uniform field. However, in the cytometer, the volume fraction is high (>40%) and the electric field is non-uniform. The geometry of the system makes it difficult to calculate an accurate value for the volume fraction ($\Phi$) in the mixture equation. In a previous work [80] it was shown that the mixture equation when used with a corrected volume fraction (to take into account the non-uniform field effect) can provide a good analytical approximation for the impedance spectrum of a single particle in suspension. The corrected volume fraction is modified by the cell constant of the cytometer, derived by using the Schwarz–Christoffel mapping

$$\Phi = \frac{4}{3}\pi R^3 \frac{1}{\kappa w l h} \tag{20}$$

with

$$\kappa = \frac{K(k)}{K'(k)} \qquad k = \tanh\left(\frac{\pi w}{2h}\right),$$

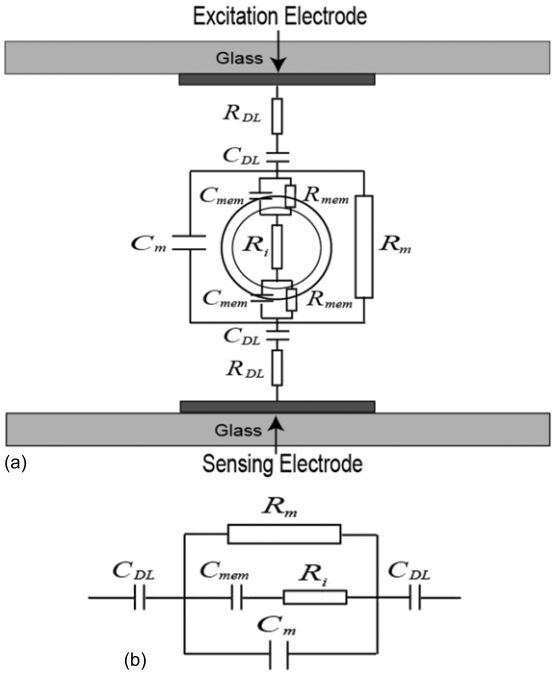


**Figure 2.** (*a*) The ECM for a cell suspended between a pair of microelectrodes. $R_{\mathrm{DL}}$ and $C_{\mathrm{DL}}$ represent the resistance and capacitance of the EDL, $R_m$ and $C_m$ the resistance and capacitance of the medium, $R_{\mathrm{mem}}$ and $C_{\mathrm{mem}}$ the resistance and capacitance of the cell membrane and $R_{\mathrm{i}}$ the resistance of the cytoplasm. (*b*) The simplified ECM, neglecting the EDL resistance and the membrane resistance.

where $\kappa$ is the cell constant, dependent on the geometrical parameters of the cytometer, $h$ is the height of the channel, $w$ is the width and $l$ is the electrode length. $K(k)$ is the complete elliptic integral of the first kind, $K'(k)$ is the complementary integral and $k$ is the modulus of the elliptic function.

Then, the complex impedance of the system, $\tilde{Z}_{\mathrm{mix}}$, becomes

$$\tilde{Z}_{\mathrm{mix}} = \frac{1}{\mathrm{j}\omega\tilde{\varepsilon}_{\mathrm{mix}} l\kappa}. \tag{21}$$

For a cell in suspension between two parallel facing electrodes, an equivalent circuit can be constructed as shown in figure 2(*a*) [27,33,82]. In this circuit, the cell is represented by a capacitor in series with a resistor, in parallel with the two elements representing the suspending medium. At low frequencies, the thin cell membrane gives rise to a large capacitance. As the frequency increases, the reactive component of this element tends to zero and the cell internal properties are represented by the resistor. In this circuit the membrane is assumed to have an extremely high resistance and the cytoplasmic capacitance is ignored. All the circuit elements are functions of the volume fraction or cell size.

The electrical double layer (EDL) [91–93] has an influence on the measurements at low frequencies (below 1 MHz for high conductivity solutions). This is generally modelled as a constant phase angle (CPA), represented by a resistor ($R_{\mathrm{DL}}$) and capacitor ($C_{\mathrm{DL}}$) in series. As shown in figure 2(*a*), the double layer is in series with the network model. A simplified model (figure 2(*b*)) was adopted for simulation in PSpice, in this case the double layer is assumed to be purely capacitive ($C_{\mathrm{DL}}$), with a value given by the product of the inverse Debye length and the permittivity of the medium.

The simplified circuit in figure 2(*b*) shows that at very low frequencies, current flow is blocked by the double layer capacitor; only the impedance of the double layer is measured. As the frequency increases, this capacitor is gradually short-circuited and the excitation voltage charges the cell in suspension. It takes a finite amount of time to charge the membrane through the extracelluar and intracellular fluid; this results in two dielectric dispersions in the radio-frequency range (between 1 and 100 MHz). The dominant dispersion at the lower frequency was termed the $\beta$-dispersion by Schwan [24]. Zhang *et al* termed both dispersions *P* and *Q*, respectively [94]. The lower frequency dispersion is governed by polarization of the cell membrane and measurement of this parameter provides information about the dielectric properties of the membrane. The second higher frequency dispersion is governed by the polarization of the cytoplasm and the suspending medium as the membrane is short circuited at these frequencies. This second dispersion is generally small and difficult to measure using impedance spectroscopy techniques. However, this dispersion is clearly visible in both DEP and ROT spectra, with distinct characteristic time constants [95–97].

The values for the individual electrical components are as follows:

$$R_{\mathrm{m}} = \frac{1}{\sigma_{\mathrm{m}}(1 - 3\Phi/2)l\kappa}, \tag{22}$$

$$C_{\mathrm{m}} = \varepsilon_{\infty} l\kappa, \tag{23}$$

$$C_{\mathrm{mem}} = \frac{9\Phi R C_{\mathrm{mem},0}}{4}\kappa l, \tag{24}$$

$$R_{\mathrm{i}} = \frac{4\left(\frac{1}{2\sigma_{\mathrm{m}}} + \frac{1}{\sigma_{\mathrm{i}}}\right)}{9\Phi\kappa l} \tag{25}$$

with

$$C_{\mathrm{mem},0} = \varepsilon_{\mathrm{mem}}/d, \tag{26}$$

$$\varepsilon_{\infty} = \varepsilon_{\mathrm{m}}\frac{2\varepsilon_{\mathrm{m}} + \varepsilon_{\mathrm{i}} - 2\Phi(\varepsilon_{\mathrm{m}} - \varepsilon_{\mathrm{i}})}{2\varepsilon_{\mathrm{m}} + \varepsilon_{\mathrm{i}} + \Phi(\varepsilon_{\mathrm{m}} - \varepsilon_{\mathrm{i}})}, \tag{27}$$

where $C_{\mathrm{mem},0}$ is the specific membrane capacitance (capacitance per unit area) and $\varepsilon_{\infty}$ is the permittivity at infinite frequency.

In these equations, the volume fraction (equation (20)) is corrected to take into account the non-uniform field configuration [98]. Ignoring the double layer, the total impedance of the circuit is

$$\tilde{Z}_{\mathrm{mix}} = \frac{R_{\mathrm{m}}(1 + \mathrm{j}\omega R_{\mathrm{i}} C_{\mathrm{mem}})}{\mathrm{j}\omega R_{\mathrm{m}} C_{\mathrm{mem}} + (1 + \mathrm{j}\omega R_{\mathrm{i}} C_{\mathrm{mem}})(1 + \mathrm{j}\omega R_{\mathrm{m}} C_{\mathrm{m}})}. \tag{28}$$

Equations (22)–(27) are versions of the MMT for a single shell cell model. The magnitude of the impedance ($\tilde{Z}_{\mathrm{mix}}$), calculated using mixture theory (equation (21)) or equation (28), is shown in figure 3(*a*). Calculations were performed with the following parameters: $\varepsilon_o = 8.854 \times 10^{-12}\,\mathrm{F\,m^{-1}}$, $d = 5\,\mathrm{nm}$, $\varepsilon_{\mathrm{m}} = 80\varepsilon_o$, $\sigma_{\mathrm{m}} = 1.6\,\mathrm{S\,m^{-1}}$, $\varepsilon_{\mathrm{mem}} = 11.3\varepsilon_o$, $\sigma_{\mathrm{mem}} = 10^{-8}\,\mathrm{S\,m^{-1}}$, $\varepsilon_{\mathrm{i}} = 60\varepsilon_o$, $\sigma_{\mathrm{i}} = 0.6\,\mathrm{S\,m^{-1}}$, with geometric dimension $w = h = l = 20\,\mu\mathrm{m}$. The calculations are performed for three sizes of cells ($r = 1, 3, 5\,\mu\mathrm{m}$), and show good agreement between mixture theory and the circuit model analysis for small cell size.

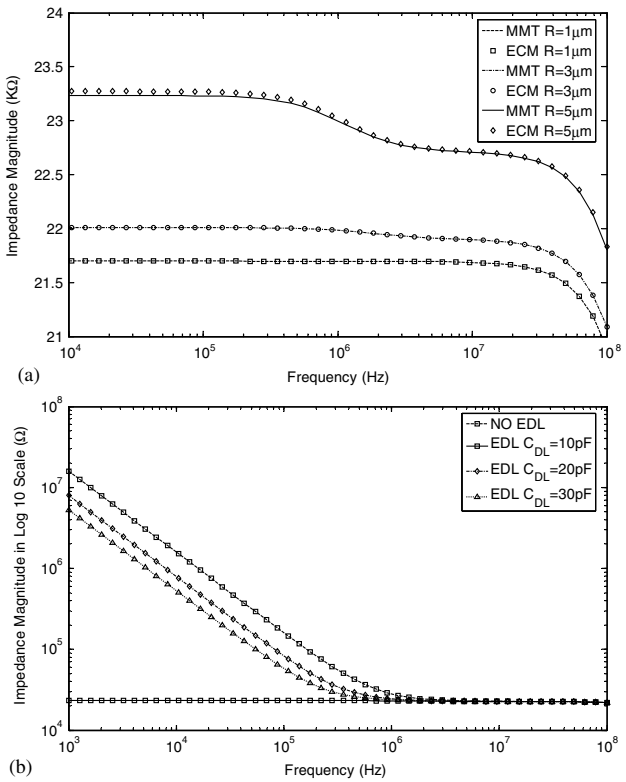


**Figure 3.** (*a*) Comparison of the impedance spectra calculated using the ECM and MMT for cells of varying size $R = 1, 3$ and $5\,\mu$m, using the single shell cell model. (*b*) Simulation of the influence of the electrical double layer (EDL) on the impedance measurements performed on a $5\,\mu$m model cell.

As the cell size increases, the difference between both models increases. This is because the circuit model ignores the membrane conductivity and also the capacitance of the cytoplasm.

Including the effect of the double layer, equation (28) becomes

$$\tilde{Z}_{\mathrm{mix\_DL}} = \frac{1}{\mathrm{j}\omega C_{\mathrm{DL}}} + \frac{R_{\mathrm{m}}(1+\mathrm{j}\omega R_{\mathrm{i}} C_{\mathrm{mem}})}{\mathrm{j}\omega R_{\mathrm{m}} C_{\mathrm{mem}} + (1+\mathrm{j}\omega R_{\mathrm{i}} C_{\mathrm{mem}})(1+\mathrm{j}\omega R_{\mathrm{m}} C_{\mathrm{m}})}. \tag{29}$$

Figure 3(*b*) shows an impedance plot for a $5\,\mu$m cell plotted from equation (29). This plot shows that the low frequency response is dominated by the double layer and that increasing the capacitance of the double layer diminishes this effect. Practically this is achieved by making electrodes with a large effective surface area. A variety of experimental and/or mathematical correction methods to reduce the effect of the double layer have been reported [91–93]. Platinum black or other nano-porous films (e.g. iridium oxide, titanium nitride) can be used to increase the effective area of the electrode surface [99, 100].

The circuit level simulation of the system was performed using PSpice in Orcad. The ECMs for the differential amplification circuit, the micro-electrodes and the cell were used to calculate the effect of variations in the properties of the cell (specific membrane capacitance and cytoplasm conductivity), while other parameters are held invariant: $R = 3\,\mu$m, $\varepsilon_{\mathrm{m}} = 78\varepsilon_o$, $\sigma_{\mathrm{m}} = 1.6\,\mathrm{S\,m^{-1}}$, $\varepsilon_{\mathrm{i}} = 60\varepsilon_o$, $C_{\mathrm{DL}} = 58\,\mathrm{pF}$. Figures 4(*a*) and (*b*) show the influence on the output spectra (real and imaginary part of the output voltage, respectively) by varying the specific membrane capacitance. Figures 4(*c*) and (*d*) show the influence on the spectra (real and imaginary part of the output voltage) by varying the cytoplasm conductivity.

### *3.3. Experimental results*

Human RBCs were used as they represent an easily accessible source of particles with broadly homogeneous and well characterized dielectric properties. Samples were obtained and handled as follows: $5\,\mu$l of whole blood (obtained from a finger prick) was suspended in 1 ml of (phosphate buffered saline) PBS. The cells were washed in PBS (i.e. centrifuged and re-suspended) to remove plasma and platelets. The cell suspension was re-suspended in PBS to give particle concentrations of $\sim 5\times10^5$ cells per ml. These samples contain both RBCs and white blood cells (WBCs); however, the ratio of RBCs to WBCs in human blood is typically 1000 : 1 and it is therefore assumed that the presence of the WBCs can be ignored.

The cells were suspended in PBS (conductivity $= 1.6\,\mathrm{S\,m^{-1}}$), introduced into the device and flowed through the microfluidic channel under the influence of an applied positive pressure at a flow velocity of $\sim$20 mms$^{-1}$. Measurements were obtained at a number of different frequency points by averaging the data from 2000 cells per frequency point. The measurement frequency was varied in a step-wise manner in the range 100 kHz–10 MHz and the applied signal amplitude was 0.5 Vpp. Full details of the experimental set-up can be found elsewhere [69, 70, 80].

Figure 5 shows an impedance spectrum for human RBCs compared with simulation from PSpice. The real and imaginary parts of the output voltage in the circuit simulation correspond to the in-phase (x-component) and the out of-phase (y-component) signal of the Lock-in amplifiers in the experiment, respectively. The data is the mean of the measurements from the cells at each frequency point. The detection region of the device was modelled using equation (22)–(27) and the PSpice models for each of the active elements (operational amplifiers, etc) were obtained from the manufacturers. Parasitic elements were also included in the model and we approximate the geometry of the RBC to that of a sphere of radius $3\,\mu$m.

In order to determine the confidence of the simulation fitting result, we use the regression coefficient defined as [42]

$$\rho = 1 - \left[\frac{\sum_{\mathrm{i}}\left(X_{\mathrm{exp}}(f_{\mathrm{i}}) - X_{\mathrm{fit}}(f_{\mathrm{i}})\right)^2}{\sum_{\mathrm{i}}\left(X_{\mathrm{exp}}(f_{\mathrm{i}})\right)^2}\right], \tag{30}$$

where $X_{\mathrm{exp}}(f_{\mathrm{i}})$ is the experimental data at certain frequency and $X_{\mathrm{fit}}(f_{\mathrm{i}})$ is the simulation fitting data at the corresponding frequency. Figure 5 shows the best fit between the experiment data and circuit simulation results for the spectra of single RBCs. The specific membrane capacitance is $8.7\,\mathrm{mF\,m^{-2}}$ and the cytoplasm conductivity is $0.62\,\mathrm{S\,m^{-1}}$ with the regression coefficients at 0.9723, ($\rho_{\mathrm{real}} = 0.9723$) for the in-phase (real part) signal and 0.9587($\rho_{\mathrm{imag}} = 0.9587$) for the out of-phase (imaginary part) signal.

From the figure it can be seen that the simulation agrees well with the experimental data for the 3 decades of frequency measured.

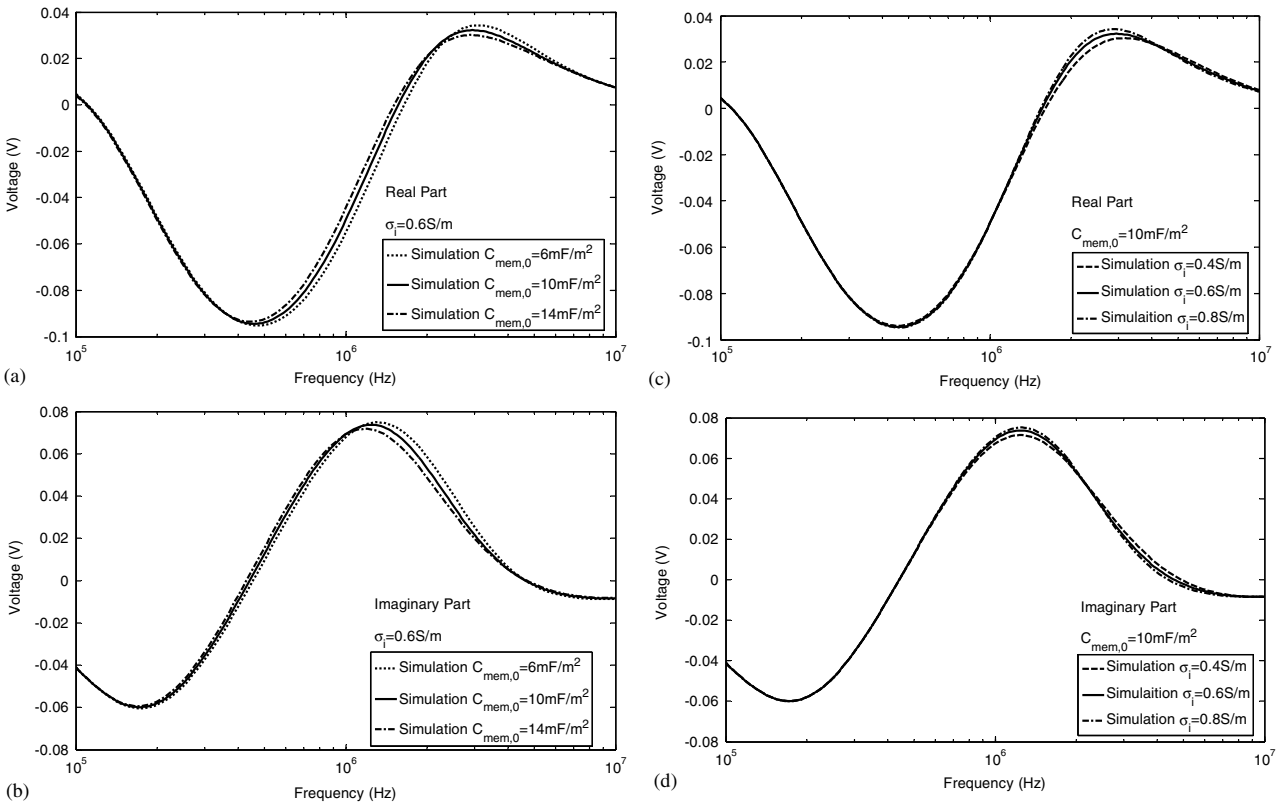


**Figure 4.** (*a*) The variation of the real part of the output signal with changes in the specific membrane capacitance of the cell, with all other parameters are held constant. (*b*) The variation of the imaginary part of the output signal with changes in the specific membrane capacitance of the cell, with all other parameters are held constant. (*c*) The variation of the real part of the output signal with changes in the cytoplasmic conductivity of the cell, for a specific membrane capacitance of $10\,\mathrm{mF\,m^{-2}}$; all other parameters held are constant. (*d*) The variation of the imaginary part of the output signal with changes in the cytoplasmic conductivity of the cell, for a specific membrane capacitance of $10\,\mathrm{mF\,m^{-2}}$; all other parameters are held constant.

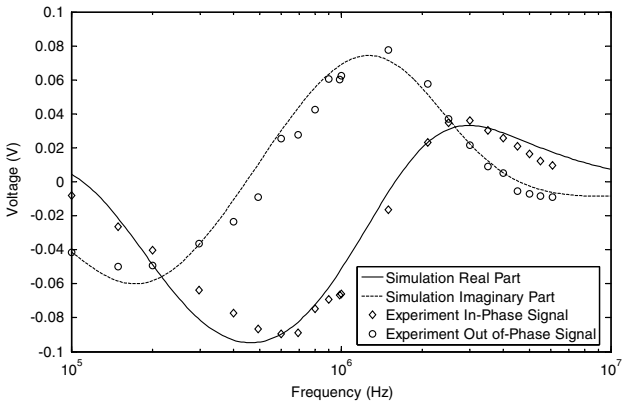


**Figure 5.** Comparison of the experimental data obtained from the micro cytometer and simulation. The in-phase and out-of phase output voltage spectra are shown for RBC in the frequency range 100 KHz–10 MHz. The solid and dashed lines are the best fit circuit simulation results for the experiment data, giving values of $C_{\mathrm{mem},0} = 8.7\,\mathrm{mF\,m^{-2}}$ and $\sigma_{\mathrm{i}} = 0.62\,\mathrm{Sm^{-1}}$ ($\rho_{\mathrm{real}} = 0.9723$ and $\rho_{\mathrm{imag}} = 0.9587$).

## 4. Conclusion

In this work we have shown that impedance spectroscopy can be used to measure the dielectric properties of single cells and that the cell can be modelled using a simple ECM comprised of linear elements. Measurements of single cells were performed at high speed using a microfabricated flow cytometer at a number of discrete frequencies. Although this method allows analysis of cell characteristics, it does not enable broad band multi-frequency analysis of cells. A multi-frequency measurement system has been reported by Fuller *et al* [101], in which discrete mixers, filters and direct digital signal synthesis circuitry was employed. Using mixed digital and analogue application-specific integrated circuits (ASICs), the system can measure up to eight frequencies simultaneously. However, this technique increases the complexity of the mixed-signal detection circuitry, and the number of frequencies is still limited. Complete broad band analysis would allow complete analysis of particle properties. One method, patented by Liu *et al* [102] is a pulsed-FFT measurement technique. However, Fuller *et al* [101] pointed out a drawback with this technique. Since the energy of the excitation signal is spread across a wide band of frequencies, rather than concentrated at a single measurement frequency, the signal-to-noise ratio of the system is much worse than a discrete frequency system. We are currently developing a new multi-frequency measurement technique, which overcomes the drawback of the pulse-FFT method, using a pseudorandom signal generated by a maximum length sequence (MLS) system. This technique promises to be capable of measuring the complete transfer function of the system, with the added advantage of low hardware cost, fast speed, high frequency resolution and excellent noise immunity.

## Acknowledgments

The authors wish to thank Andrew Whitton for assistance with microfabrication. They also thank the staff of the CMI at EPFL, Switzerland. This work was funded by EPSRC under Project Number GR/R28942.

## Reference

[1] Höber R 1910 Eine Methode die elektrische Leitfaehigkeit im Innern von Zellenzu messen *Arch. Ges. Physiol.* **133** 237–59
[2] Höber R 1912 Ein zweites Verfahren die Leitfaehigkeit im Innern von Zellen ze messem *Arch. Ges. Physiol.* **148** 189–221
[3] Höber R 1913 Messungen der inneren Leitfaehigkeit von Zelen III *Arch. Ges. Physiol.* **150** 15–45
[4] Fricke H 1924 A mathematical treatment of the electrical conductivity of colloids and cell suspensions *J. Gen. Physiol.* **6** 375–84
[5] Fricke H 1924 A mathematical treatment of the electric conductivity and capacity of disperse systems: I. The electric conductivity of a suspension of homogeneous spheroids *Phys. Rev.* **24** 575–87
[6] Fricke H 1924 The electric conductivity of disperse systems *J. Gen. Physiol.* **6** 741–6
[7] Fricke H and Morse S 1925 An experimental study of the electrical conductivity of disperse systems: I. Cream *Phys. Rev.* **25** 361–7
[8] Fricke H 1925 A mathematical treatment of the electric conductivity and capacity of disperse systems: II. The capacity of a suspension of conducting membrane for a current of low frequency *Phys. Rev.* **26** 678–81
[9] Fricke H 1925 The electric capacity of suspensions of a red corpuscles of a dog *Phys. Rev.* **26** 682–7
[10] Fricke H 1925 The electric capacity of suspensions with special reference to blood *J. Gen. Physiol.* **9** 137–52
[11] Fricke H 1925 The electric resistance and capacity of blood for frequencies between 800 and 4.5 million cycles *J. Gen. Physiol.* **9** 153–67
[12] Fricke H 1931 The electric conductivity and capacity of disperse systems *Physics* **1** 106–15
[13] Maxwell J C 1954 *A Treatise on Electricity and Magnetism* (New York: Dover)
[14] Fricke H and Curtis H J 1935 The electric impedance of hemolyzed suspensions of mammalian erythrocytes *J. Gen. Physiol.* **18** 821–36
[15] Cole K S 1928 Electric impedance of suspensions of spheres *J. Gen. Physiol.* **12** 29–36
[16] Cole K S 1928 Electric impedance of suspensions of Arbacia eggs *J. Gen. Physiol.* **12** 37–54
[17] Cole K S 1932 Electric phase angle of cell membranes *J. Gen. Physiol.* **15** 641–9
[18] Cole K S 1935 Electric impedance of *Hipponoë* eggs *J. Gen. Physiol.* **18** 877–87
[19] Cole K S and Cole R H 1936 Electric impedance of *Asteria* eggs *J. Gen. Physiol.* **19** 609–23
[20] Cole K S and Cole R H 1936 Electric impedance of *Arbacia* eggs *J. Gen. Physiol.* **19** 625–32
[21] Curtis H J and Cole K S 1937 Transverse electric impedance of Nitella *J. Gen. Physiol.* **21** 189–201
[22] Cole K S and Curtis H J 1938 Electric impedance of single marine eggs *J. Gen. Physiol.* **21** 591–9
[23] Schwan H P 1999 The practical success of impedance techniques from a historical perspective *Ann. N.Y. Acad. Sci.* **873** 1-12
[24] Schwan H P 1957 Electrical properties of tissue and cell suspensions *Adv. Biol. Med. Phys.* **5** 147–209
[25] Schwan H P 1963 Electrical properties of tissue and cell suspensions *Physical Techniques in Biological Research* ed W L Nastuk (New York: Academic) **6** 323–406
[26] Pethig R and Kell D B 1987 The passive electrical properties of biological systems: their significance in physiology, biophysics and biotechnology *Phys. Med. Biol.* **32** 933–70
[27] Foster K R and Schwan H P 1989 Dielectric properties of tissues and biological materials: A Critical Review *Critical Rev. Biomed. Eng.* **17** 25–104
[28] Jones T B 1995 *Electromechanics of Particles* (Cambridge: Cambridge University Press)
[29] Zimmermann U, Friedrich U, Mussauer H, Gessner P, Hämel K and Sukhorukov V 2000 Electromanipulation of mammalian cells: fundamentals and application *IEEE Trans. Plasma Sci.* **28** 72–82
[30] Grimnes S and Martinsen Ø G 2000 *Bioimpedance Bioelectricity and Basics* (New York: Academic)
[31] Gascoyne P R C and Vykoukal J 2002 Particle separation by dielectrophoresis *Electrophoresis* **23** 1973–83
[32] Asami K 2002 Characterization of heterogeneous systems by dielectric spectroscopy *Prog. Polym. Sci.* **27** 1617–59
[33] Morgan H and Green N G 2003 *AC Electrokinetics: Colloids and Nanoparticles* (Baldock, Hertfordshire, England: Research Studies Press Ltd.)
[34] Feldman Yu, Ermolina I and Hayashi Y 2003 Time domain dielectric spectroscopy study of biological systems *IEEE Trans. Dielectr. Electr. Insul.* **10** 728–53
[35] Weaver J C 2003 Electroporation of biological membranes from multicellular to nano scales *IEEE Trans. Dielectr. Electr. Insula* **10** 754–768
[36] K'Owino I O and Sadik O A 2005 Impedance spectroscopy: A powerful tool for rapid biomolecular screening and cell culture monitoring *Electroanalysis* **17** 2101–13
[37] Ramos A, Morgan H, Green N G and Castellanos A 1998 AC electrokinetics: a review of forces in microelectrode structures *J. Phys. D: Appl. Phys.* **31** 2338–53
[38] Green N G, Ramos A and Morgan H 2000 AC elelectrokinetcis: a survey of sub-micrometer particle dynamics *J. Phys. D: Appl. Phys.* **33** 632–41
[39] Green N G and Morgan H 1999 Dielectrophoresis of submicrometer latex spheres: 1. Experimental results *J. Phys. Chem.* B **103** 41–50
[40] Hughes M P and Morgan H 1999 Dielectrophoretic characterization and separation of antibody-coated submicrometer latex spheres *Anal. Chem.* **71** 3441–5
[41] Ermolina I and Morgan H 2005 The electrokinetic properties of latex particles: comparison of electrophoresis and dielectrophoresis *J. Colloid Interface Sci.* **285** 419–28
[42] Chan K L, Morgan H, Morgan E, Cameron I T and Thomas M R 2000 Measurements of the dielectric properties of peripheral blood mononuclear cells and trophoblast cells using AC electrokinetic techniques *Biochim. Biophys. Acta* **1500** 313–22
[43] Huang Y, Hölzel R, Pethig R and Wang X-B 1992 Differences in the ac electrodynamics of viable and non-viable yeast cells determined through combined dielectrophoresis and electrorotation studies *Phys. Med. Biol.* **37** 1499–517
[44] Pohl H A 1978 *Dielectrophoresis* (Cambridge: Cambridge University Press)
[45] Pethig R, Huang Y, Wang X-B and Burt J P H 1992 Positive and negative dielectrophoretic collection of colloidal particles using interdigitated castellated microelectrodes *J. Phys. D: Appl. Phys.* **24** 881–8
[46] Cruz J M and Gracia-Diego F J 1998 Dielectrophoretic motion of oblate spheroidal particles. Measurements of motion of red blood cells using the stokes method *J. Phys. D: Appl. Phys.* **31** 1745–51
[47] Pethig R, Bressler V, Carswell-Crumption C, Chen Y, Foster-Haje L, Garcia-Ojeda M E, Lee R S, Lock G M, Talary M S and Tate K M 2002 Dielectrophoretic studies of the activation of human T lymphocytes using a newly developed cell profiling system *Electrophoresis* **23** 3057–2063
[48] Hughes M P, Morgan H and Rixon F J 2002 Measuring the dielectric properties of herpes simplex virus type I virions

with dielectrophoresis *Biochim. Biophys. Acta* **1571** 1–8
[49] Lapizco-Encinas, Simmoms B A, Cummings E B and Fintschenko Y 2004 Insulator-based dielectrophoresis for the selective concentration and separation of live bacteria in water *Electophoresis* **25** 1695–704
[50] Sauer F A and Schlögl R W 1985 *Interactions between Electromagnetic Fields and Cells* ed A Chiabrera *et al* (New York: Plenum) pp 203–51
[51] Archer S, Morgan H and Rixon F J 1999 Electrorotation studies of baby hamster kidney fibroblasts infected with herpes simplex virus type 1 *Biophys. J.* **76** 2833–42
[52] Ziervogel H, Glaser R, Schadow D and Heymann S 1986 Electrorotation of Lymphocytes- the influence of membrane events and nucleus *Biosci. Rep.* **6** 973–82
[53] Turcu I and Lucaciu C M 1989 Electrorotation: a spherical shell model *J. Phys. A: Math. Gen.* **22** 995–1003
[54] Hölzel R 1997 Electrorotation of single yeast cells at frequencies between 100 Hz and 1.6 GHz *Biophys. J.* **73**, 1103–9
[55] Yang J, Huang Y, Wang X-J, Wang X-B, Becker F F and Gascoyne P R C 1999 Dielectric properties of human leukocytes subpopulations determined by electrorotation as a cell separation criterion *Biophys. J.* **76** 3307–14
[56] Huang J P, Yu K W, Gu G Q and Karttunen M 2003 Electrorotation in graded colloidal suspensions *Phys. Rev.* E **67** 1–5
[57] Dalton C, Goater A D, Burt J P H and Smith H V 2004 Analysis of parasites by electrorotation *J. Appl. Microbiol.* **96** 24–32
[58] Gimsa J, Marszalek P, Loewe U and Tsong T Y 1991 Dielectrophoresis and electrorotation of neurospora slime and murine myeloma cells *Biophys. J.* **60** 749–60
[59] Wang X-B, Pethig R and Jones T B 1992 Relationship of dielectrophoretic and electrorotational behaviour exhibited by polarized particles *J. Phys. D: Appl. Phys.* **25** 905–12
[60] Huang Y, Wang X-B, Becker F and Gascoyne P R C 1996 Membrane changes associated with the temperature-sensitive P85$^{gag\text{-}mos}$-dependent transformation of rat kidney cells as determined by dielectrophoresis and electrorotation *Biochim. Biophys. Acta* **1282** 76–84
[61] Goater A D and Pethig R 1998 Electrorotation and dielectrophoresis *Parasitology* **116** 177–89
[62] Gimsa J 2001 A comprehensive approach to electro-orientation, electrodeformation, dielectrophoresis and electrorotation of ellipsoidal particles and biological particles *Bioelectrochemistry* **54** 23–31
[63] Reuss O R, Kurschner M, Dilsky S, Horbaschek M, Schenk W A, Zimmerman U and Sukhorukov V L 2002 Interaction of fluorinated lipophilic ions with the plasma membrane of mammalian cells studied by electrorotation and dielectrophoresis *J. Electrostat.* **56** 419–34
[64] Maxwell J C 1954 *A Treatise on Electricity and Magnetism* (New York: Dover)
[65] Foster K R, Sauer F A and Schwan H P 1992 Electrorotation and levitation of cells and colloidal particles *Biophys. J.* **63** 180–90
[66] Wang X-B, Huang Y, Holzel R, Burt J P H and Pethig R 1993 Theoretical and experimental investigations of the interdependence of the dielectric. Dielectrophoretic and electrorotational behaviour of colloidal particles *J. Phys. D: Appl. Phys.* **26** 312–22
[67] Becker F F, Wang X-B, Huang Y, Pethig R, Vykoukal J and Gascoyne P R C 1995 Separation of human breast cancer cells from blood by differential dielectric affinity *Proc. Natl. Acad. Sci. USA* **92** 860–4
[68] Holmes D, Morgan H and Green N G 2006 High throughput particle analysis: Combing dielectrophoretic particle focussing with confocal optical detection *Biosens. Bioelectron.* **21** 1621–30
[69] Gawad S, Schild L and Renaud Ph 2001 Micromachined impedance spectroscopy flow cytometer for cell analysis and particle sizing *Lab Chip* **1** 76–82
[70] Morgan H, Holmes D and Green N G 2006 High speed simultaneous single particle impedance and fluorescence analysis on a chip *Curr. Appl. Phys.* **6** 367-370
[71] Coulter W H 1956 High speed automatic blood cell counter and cell analyzer *Proc. Natl. Electron. Conf.* **12** 1034–40
[72] Hoffman R A and Britt W R 1978 Flow-system measurement of cell impedance properties *J. Histochem. Cytochem.* **27** 234–40
[73] Hoffman R A, Johnson T S and Britt W R 1981 Flow cytometric electronic direct current volume and radiofrequency impedance measurements of single cells and particles *Cytometry* **1** 377–84
[74] Nelson M 1999 An overview of the use of flow cytometry in the analysis of mixed red cell populations *Pathology* **31** 191–8
[75] Suehiro J, Yatsunami R, Hamada R and Hara M 1999 Quantitative estimation of biological cell concentration suspended on aqueous medium by using dielectrophoretic impedance measurement method *J. Phys. D: Appl. Phys.* **32** 2814–20
[76] Ayliffe H E, Frazier A B and Rabbit R D 1999 Electric impedance spectroscopy using microchannels with integrated metal electrodes *IEEE Microelectromech. Sys.* **8** 50–7
[77] Sohn L L, Saleh O A, Facer G R, Beavis A J, Allan R S and Notterman D A 2000 Capacitance cytometry: measuring biological cells one by one *Proc. Natl. Acad. Sci. USA* **97** 10687–90
[78] Yao B, Luo G A, Feng X, Wang W, Chen L X and Wang Y M 2004 A microfluidic device based on gravity and electric force driving for flow cytometry and fluorescence activated cell sorting *Lab Chip* **4** 603–7
[79] Palková Z, Váchová L, Valer M and Preckel T 2004 Single-cell analyis of yeast, mammalian cells and fungal spores with a microfluidic pressure-driven chip-based system *Cytometry* A **59** 246–53
[80] Gawad S, Cheung K, Seger U, Bertsch A and Renaud Ph 2004 Dielectric spectrosopy in a micromachined flow cytometer: theoretical and practical considerations *Lab Chip* **4** 241–51
[81] Holmes D, Sandison M E, Green N G and Morgan H 2005 On-chip high-speed sorting of micron-sized particles for high-throughput analysis *IEE Proc. Nanobiotechnol.* **152** 129–35
[82] Cheung K, Gawad S and Renaud Ph 2005 Impedance spectroscopy flow cytometer: on-chip label-free cell differentiation *Cytometry* A **65** 124–32
[83] Tang H and Gao Y F 2005 An impedance microsensor with coplanar electrodes and vertical sensing apertures *IEEE Sensors* **5** 1346–52
[84] Cho Y H, Yamamoto T, Sakai Y, Fujii T and Kim B 2006 Development of microfluidic device for electrical/physical characterization of single cell *J. Microeletromech. Sys.* **15** 287-295
[85] Schwan H P, Takashima S, Miyamoto V K and Stoeckenius W 1970 Electrical properties of phospholipid vesicles *Biophys. J.* **10** 1102–19
[86] Gimsa J and Wachner D 1998 A unified resistor-capacitor model for impedance, dielectrophoresis, electrorotation and induced transmembrane potential *Biophys. J.* **75** 1107–16
[87] Sekine K 2000 Application of boundary element method to calculation of the complex permittivity of suspensions of cells in shape of $D_{\infty h}$ symmetry *Bioelectrochemistry* **52** 1–7
[88] Gowrishankar T R and Weaver J C 2003 An approach to electrical modeling of single and multiple cells *Proc. Natl. Acad. Sci. USA* **100** 3203–8
[89] Stewart D A Jr, Gowrishankar T R, Smith K C and Weaver J C 2005 Cylindrical cell membranes in uniform applied electric fields: validation of a transport lattice method *IEEE Trans. Biomed. Eng.* **10** 1643–53

[90] Asami K 2006 Dielectric dispersion in biological cells of complex geometry simulated by the three-dimensional finite difference method *J. Phys. D: Appl. Phys.* **39** 492–9

[91] Feldman Yu, Nigmatullin R, Polygalov E and Texter J 1998 Fractal-polarization correction in time domain dielectric spectroscopy *Phys. Rev.* E **58** 7561–5

[92] Feldman Yu, Polygalov E, Ermolina I, Polevaya Yu and Tsentsiper B 2001 Electrode polarization correction in time domain dielectric spectroscopy *Meas. Sci. Technol.* **12** 1355–64

[93] Bordi F, Cametti C and Gili T 2001 Reduction of the contribution of electrode polarization effects in the radiowave dielectric measurements of highly conductive biological cell suspensions *Bioelectrochemistry* **54** 53–61

[94] Zhang H Z, Sekine K, Hanai T and Koizumi N 1983 Dielectric observations on polystyrene microcapsules and the theoretical analysis with reference to interfacial polarization *Colloid Polymer. Sci.* **261** 381–9

[95] Pauly H and Schwan H P 1959 Uber die Impedanz einer Suspension von kugelformigen Teilchen mit einer Schale *Z. Naturforsch* **B14** 125

[96] Kotnik T, Miklavcic D and Slivnik T 1998 Time course of transmembrane voltage induced by time-varying electric fields—a method for theoretical analysis and its application *Bioelectrochem. Bioenerg.* **45** 3–16

[97] Sun T, Gawad S, Green N G and Morgan H 2007 Dielectric spectroscopy of single cells; time domain analysis using Maxwell's mixture equation *J. Phys. D: Appl. Phys.* **40** 1 (this issue)

[98] Gawad S 2004 Dielectric spectroscopy in a microfabricated flow cytometer *PhD Thesis* Lausanne EPFL, Switzerland

[99] Evans S A, Elliott J M, Andrews L M, Bartlett P N, Doyle P J and Denuault G 2002 Detection of hydrogen peroxide at mesoporous platinum microelectrodes *Anal. Chem.* **74** 1322–6

[100] Honda K, Rao T N, Tryk D A, Fujishima A, Watanabe M, Yasui K and Masuda H 2001 Impedance characteristics of the nanoporous honeycomb diamond electrodes for electrical double-layer capacitor applications *J. Electrochem. Soc.* **148** A668–79

[101] Fuller C K, Hamilton J, Ackler H, Krulevitch P, Boser B, Eldredge A, Becker F, Yang J and Gascoyne P 2000 Microfabricated multi-frequency particle impedance characterization system *Proc. μTAS Symp. (Enschede, The Netherlands, May 2000)* pp 265–8

[102] Liu Y, Abel W, Janette J, Belch F and Tweedie R J 1997 *US Patent* 5,691,633